Observation of dark photovoltaic spatial solitons

Minoru Taya,[1] Matthew C. Bashaw,[2] M. M. Fejer,[1] Mordechai Segev,[3] and George C. Valley[4]
[1]*Department of Applied Physics and Center for Nonlinear-Optical Materials, Stanford University, Stanford, California 94305*
[2]*Department of Electrical Engineering and Center for Nonlinear-Optical Materials, Stanford University, Stanford, California 94305 and Silicon Valley Photonics, Menlo Park, California 94025*
[3]*Department of Electrical Engineering, Center for Photonics and Optoelectronic Materials, and the Princeton Material Institute, Princeton University, Princeton, New Jersey 08544*
[4]*Hughes Research Laboratories, Malibu, California 90265*
(Received 2 December 1994; revised manuscript received 5 June 1995)

We report on the observation of planar dark spatial solitons due to the bulk photovoltaic effect in lithium niobate, with intensities of the order of 10 W/cm^2 and widths of approximately 20 μm. Photovoltaic solitons display a characteristic tensorial dependence on their direction of propagation, on their polarization, and on the orientation of the amplitude profile, with respect to the principal axes of the crystalline medium. The index perturbation associated with a dark soliton persists in the dark, and it can trap and guide a second beam.

PACS number(s): 42.65.Jx, 42.50.Rh, 42.65.Hw

Spatial solitons arising from the self-guiding of light beams in Kerr and Kerr-like media have been investigated for three decades. A bright soliton, in which a beam of light propagates without change in its transverse profile, occurs when self-focusing due to the light-induced change in the index of refraction balances diffraction [1–5]; in Kerr media, the resulting *positive* index perturbation is proportional to the intensity of the beam. A dark soliton, in which a dark band, or notch, is superimposed on an otherwise uniform background illumination, occurs when *self-defocusing* due to a light-induced index change balances the diffraction of the notch [6–8]; in Kerr media, the resulting *negative* index perturbation is proportional to the intensity of the beam. A dark soliton may be black, in which the intensity minimum is zero, or gray, in which it is nonzero but less than the background intensity [6,9]. Recent theoretical investigations have also considered the case of saturable Kerr-like nonlinearities and have predicted the existence of solitons in this regime [10–12].

We report here the observation of photovoltaic spatial solitons, which are predicted to occur in a medium with a significant photovoltaic effect [13]. The optical nonlinearity responsible for soliton formation is due to the transport of electronic charge dominated by the bulk photovoltaic (photogalvanic) currents. Electrons are photoexcited from impurity centers with momentum preferentially directed along the c axis of a ferroelectric crystal, and are then trapped in different impurity centers. The resulting space-charge distribution gives rise to an index gradient through the electro-optic effect. This index gradient is responsible for the self-guiding needed to generate photovoltaic solitons. We examine here $LiNbO_3$, for which the photovoltaic effect results in a negative index perturbation capable of supporting dark solitons. We investigate the specific case of dark planar photovoltaic solitons, in which a dark notch is trapped in one transverse dimension.

Photovoltaic solitons differ significantly from Kerr solitons. The Kerr nonlinearity is a consequence of third-order polarizability, which is represented as a fourth-rank tensor [14,15]. The tensorial properties result in a self-induced index profile that depends only on the intensity and the polarization of light. In contrast, the photovoltaic nonlinearity results from charge transport and is governed by the polarization of the incident light, the third-rank photovoltaic tensor, the third-rank Pockels tensor, and the gradient of the intensity profile. Consequently, the self-induced index profile depends not only on the intensity and polarization of light, as do Kerr solitons, but also on the specific orientation of the intensity profile, as Kerr solitons do not. We describe here a number of distinct features of planar photovoltaic solitons that arise from these properties. For example, planar solitons can be supported only when a component of the gradient of the optical intensity is oriented along the c axis, but cannot be supported when illumination is uniform in this direction. Furthermore, because the physical mechanism responsible for solitons is the separation and trapping of electronic charge, the index perturbation associated with the photovoltaic soliton persists in the dark and may be used as a waveguide to trap a beam at an insensitive wavelength.

Photovoltaic solitons are further distinct from solitons supported by photorefractive media under the influence of an applied electric field. When an applied field generates currents responsible for charge transport, at least two types of solitons are possible: Quasi-steady-state drift solitons result as a consequence of coupling between constituent plane-wave components of the light beam

[16–18]; these solitons are spatially nonlocal and occur only within a specific transient time regime, disappearing at steady state; their most distinct properties are transverse profiles independent of intensity, and self-trapping in both transverse dimensions. Screening solitons occur at steady state and stem from nonuniform screening of the applied electric field by trapped charge carriers [19–21].

In contrast to earlier observations of dark solitons in Kerr media such as gases [22,7] or semiconductors [8], photovoltaic solitons arise from a nonlinearity that saturates at sufficiently high intensities. When the background intensity is small in comparison to the intensity required to generate photoconductivity equal to the dark conductivity (equivalent dark irradiance), the index perturbation is approximately linear with intensity for a given normalized amplitude profile; in this regime, response time at room temperature is on the order of the dark dielectric relaxation time. The observations presented here are carried out in a regime where the maximal intensity of the beam (away from the dark notch) is much larger than the equivalent dark irradiance, with a response time equal to the illuminated dielectric relaxation time. The dark solitons reported here consist of dark notches on an otherwise bright beam of finite extent that does not broaden significantly along the direction of propagation [7,22].

The index perturbations can be estimated by examination of the current equation which, neglecting diffusion, can be approximated as [13]

$$\mathbf{j}=e\mu n_e\mathbf{E}+\kappa(N-N_A)I(\mathbf{r})\mathbf{c}\ , \tag{1}$$

in which $\mathbf{j}$ is the vector current density; e is the electron charge; μ is the free-electron mobility; $\mathbf{E}$ is the electric field; κ is the photovoltaic constant; N is the number of impurity centers; N_A is the number density of negatively charged acceptors that compensate for the ionized donors; $I(\mathbf{r})$ is the incident intensity at position $\mathbf{r}$; $\mathbf{c}$ is the vector orientation of the crystalline c axis; $n_e=s(I+I_d)(N-N_A)/(\gamma N_A)$ is the free-electron concentration, in which s is the photoexcitation cross section; γ is the recombination coefficient; and I_d is the dark irradiance (i.e., the intensity of light required to generate a photoconductivity equal to the dark conductivity).

To examine the dependence of the self-trapping effects on the relation between the orientations of the intensity gradient and the crystalline c axis, we consider two orientations of the dark notch in the intensity. In the first orientation, the dark notch is oriented so that its intensity gradient is parallel to the c axis [Fig. 1(a)]. When the background illumination is sufficiently broad, this case reduces to the problem of planar solitons in two dimensions: the propagation dimension and the transverse dimension [13]. In the simplest case of planar solitons described by a scalar nonlinear wave equation, when free-carrier diffusion can be neglected and the limiting space-charge field associated with the photorefractive medium is large in comparison to the characteristic photovoltaic field, we apply open-circuit boundary conditions ($\mathbf{j}=0$) and use the Pockels effect to show that the *mathematical*

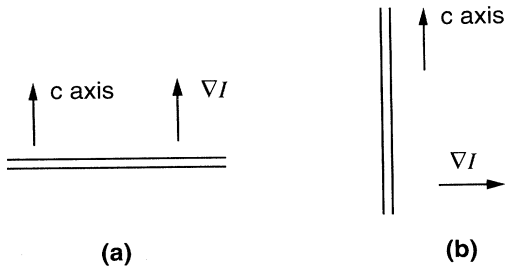

FIG. 1. Orientation with the index gradient (a) parallel to the c axis and (b) perpendicular to the c axis.

form of the nonlinear index perturbation is that of a saturable Kerr nonlinearity [13].

$$\delta n=\alpha I/(I+I_d)\ . \tag{2}$$

The constant α equals $-n_0^3 rE_p/2$, in which n_0 is the unperturbed refractive index, r is the effective electro-optic (Pockel's) coefficient, and $E_p=\kappa\Gamma/(e\mu)$ the photovoltaic field constant in which $\Gamma=\gamma N_A$ is the free-electron recombination rate. The index perturbation is linear with intensity (not saturated) only when the intensity is significantly less than the dark irradiance. For an optical field, $\mathbf{A}(x,z)\exp[i(kz-\omega t)]$, which is polarized along the c axis (x dimension) and propagates perpendicular to the c axis (z dimension), and whose intensity gradient is parallel to the c axis, the paraxial propagation equation for the slowly varying amplitude $A_x(x,z)$ is

$$\frac{\partial^2 A_x}{\partial x^2}+2ik\frac{\partial A_x}{\partial z}+\frac{2\delta n(A_x)}{n_0}k^2A_x=0 \tag{3}$$

and supports soliton solutions of the form

$$A_x\propto u(x)\exp(i\gamma z)\ . \tag{4}$$

Here, k is the wave number, ω is the frequency, $I=|A_x|^2$, and $u(x)$ is the normalized amplitude that propagates without change and a phase accumulation of γ. The amplitudes, which have been examined in detail by Valley *et al.* [13], are dark solitons whose symmetrically odd transverse spatial profiles resemble the hyperbolic tangent profile (a solution for defocusing Kerr nonlinearities), but which cannot be described by well-known analytical expressions. These solitons display the following properties: a π phase step occurs at the location of zero intensity; the width associated with the transverse profile remains constant along the direction of propagation; the self-induced refractive index perturbation associated with the dark soliton is positive in the dark region with respect to the background index in the bright region and is therefore capable of guiding a second beam (of weaker power or a less sensitive wavelength), in a manner similar to the guiding properties of dark Kerr solitons [23]; and a given observable dark soliton width can occur at two values of background intensities.

In the other orientation, the dark notch is oriented so that its intensity gradient is perpendicular to the c axis

[Fig. 1(b)]. Becuase $\nabla \times \mathbf{E}=0$ at steady state,

$$\frac{\partial E_x}{\partial y}=\frac{\partial E_y}{\partial x}\ , \tag{5}$$

in which x is the dimension along the c axis and y is the other transverse dimension. For a sufficiently broad background beam, with a narrow dark notch extending laterally to the limits of the background beam, the electric field will be approximately translationally invariant in the x dimension away from the limits, so that $\partial \mathbf{E}/\partial x$ vanishes. Therefore, $\partial E_x/\partial y=0$, so that the electric-field component along the c axis, E_x, does not vary in the direction of the intensity gradient. Away from the limits of the background beam, we find that the intensity is given by $I(y)$ (so that the photovoltaic current is oriented in the x directon but varies in the y dimension). Because the transport is symmeric about the notch in the y dimension, and because $\nabla \cdot \mathbf{j}=0$, we find that E_x is constant, and only when the effects of diffusion are included do we obtain nonvanishing E_y [13]. Diffusion fields do not cause the self-focusing or self-defocusing effects described here and are typically negligible in $LiNBO_3$ [13]. Consequently, this orientation of the incident intensity profile cannot support photovoltaic solitons. We expect these conditions to be valid for this orientation when the width of the dark notch is much less than the width of the background beam, and the corresponding electric field results in a background index change.

Thus the tensorial nature of the photovoltaic and electro-optic effects due to the noncentrosymmetric nature of $LiNbO_3$ favors soliton propagation along a direction perpendicular to the crystalline c axis, light polarized along the c axis, and the gradient of amplitude profile along the c axis [13]. In this arrangement, the electric field arising from the space-charge separation is along the c axis, so that the refractive index perturbation is proportional to the product of the strongest electro-optic tensor element ($r=r_{333}$) and the strongest photovoltaic tensor element ($\kappa=\kappa_{333}$). The refractive index perturbation requires charge transport and therefore occurs on slow time scales for $LiNbO_3$ (on the order of minutes) and modest irradiances (watts per square centimeter or less). The charge separation responsible for the self-induced index perturbation persists in the dark for a few dark decay times, which are typically the dark dielectric relaxation times (on the order of years in some $LiNbO_3$ samples).

We excite the dark soliton by introducing a phase step across a beam of circular cross section and imaging it onto the front surface of a sample $LiNbO_3$ to produce a narrow dark notch. The beam propagates perpendicular to the c axis, and the variations in phase and in intensity arising from the phase step occur along the c axis. Prior to formation of the index perturbation, the notch diffracts, becoming wider at the exit face of the crystal. As the refractive index variation associated with the soliton forms, the notch narrows at the exit face of the crystal. The resulting index perturbation forms a waveguide that can be probed by launching a second beam into it.

The experimental arrangement (Fig. 2) consists of a nominally undoped sample of congruent $LiNbO_3$, a collimated continuous-wave argon-ion laser beam of 488 nm, a glass microscope cover slip that can be adjusted by tilting to yield an arbitrary phase step across the beam, and a telescope to image the collimated beam onto the front crystal surface. All measurements are performed at room temperature. The crystal is oriented with its c axis perpendicular to the direction of the laser beam, and the beam is polarized parallel to the c axis, as described above. The beam profile is detected by a charge-coupled device array and captured by a computer-controlled frame grabber. For an average background intensity of ~ 10 W/cm^2, we obtain steady-state measurements after a 15 min exposure.

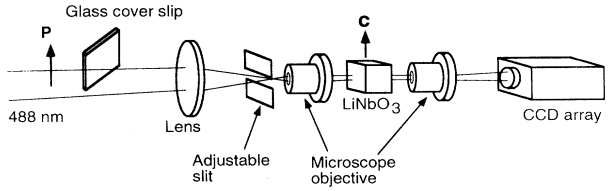

FIG. 2. Experimental arrangement.

The tensorial nature of the photovoltaic defocusing nonlinearity is illustrated in Fig. 3. A corner of a microscope cover slip is inserted into the beam path, generating both a horizontal and a vertical dark notch at the front (input) surface of the crystal. Before the formation of the index perturbation, the notches diffract similarly, as indicated by the intensity profiles at the rear (output) surface of the crystal [Fig. 3(a)]; also present are higher-order diffraction fringes. At steady state, the nonlinearity favors amplitude profile gradients oriented along the c axis. Therefore, only the width of the horizontal dark notch narrows, and the vertical notch continues to diffract [Fig. 3(b)]. The index perturbation associated with the horizontal notch is positive, and upon removal of the cover slip, the perturbation can guide a portion of a uniformly illuminating beam [Fig. 3(c)].

To generate planar solitons, an edge of the phase step generates a dark notch that is spatially filtered in the Fourier plane (to eliminate the higher orders generated by the glass cover slip) and then imaged onto the front surface of the crystal with a full width of ~ 20 μm. The power of the background beam is 20 mW, with an average intensity of 10 W/cm^2. Observation of scattered light normal to the direction of propagation allows us to observe the spatial evolution of the incident beam from the side of the crystal. The spatial and temporal evolution of the dark soliton are shown by side profiles in Fig. 4. Before the index perturbation associated with the soliton forms, normal diffraction is clearly illustrated by the widening of the input dark notch as it propagates through the medium [Fig. 4(a)]. After soliton formation the dark notch narrows within the first few millimeters of the medium, and maintains a relatively uniform profile through the remainder of the medium [Fig. 4(b)]. The width of the trapped dark notch is approximately 15 μm. Some perturbation in the width does occur as it propagates, but the perturbation is significantly smaller than the diffraction that occurs before the perturbation forms.

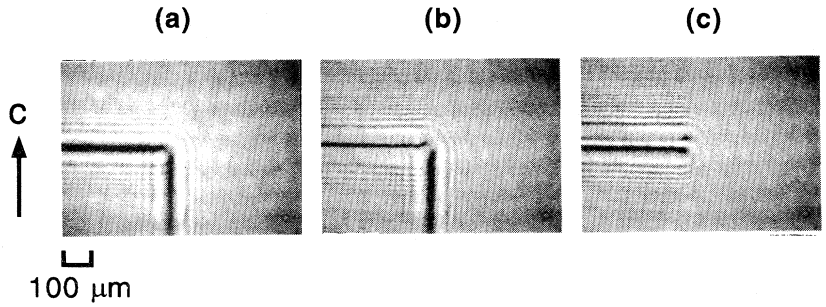

FIG. 3. Orientational behavior of dark photovoltaic solitons for a $1\times1\times1$ cm^3 sample of congruent $LiNbO_3$. The background beam diameter is ~1.4 mm and the average intensity is ~2 W/cm^2. Shown are (a) the initial intensity distribution in the output plane when the corner of the cover slip is in the beam path; (b) intensity distribution at steady state; and (c) intensity distribution after removal of the cover slip immediately after steady state.

Beyond 3 cm self-defocusing associated with the background beam becomes significant, changing the background amplitude profile and therefore, to some extent, the properties and size of the dark notch.

The data in Figs. 4(a) and 4(b) can be evaluated quantitatively by examining intensity profiles taken from the images. Because we are imaging through the volume of the medium, the profiles do not represent the light in the image plane but instead an accumulation of light scattered by the full extent of the propagating beam. The profiles may be examined to determine whether they show diffraction or behavior indicative of soliton propagation. The profiles corresponding to Fig. 4(a) are shown in Fig. 5(a), illustrating significant diffraction from the front surface of the medium. The profiles corresponding to Fig. 4(b) are shown in Fig. 5(b), illustrating that after 5 mm the propagating beam experiences little diffraction. The profiles do show some evolution of the soliton into a gray soliton.

The waveguide associated with the dark soliton can be probed by launching a second beam into it. To illustrate this property, we generate a dark soliton by 488-nm light with a dark notch. Then we use the resulting waveguide structure to guide a second beam of a different wavelength. Observation of the waveguide structure formed by the dark soliton is made with a second line of the argon laser operating at 514 nm, which enters the beam path after the phase step. Although $LiNbO_3$ is somewhat less sensitive at 514 nm than 488 nm, we examine the waveguide with the 514-nm beam for relatively brief time intervals (seconds) to avoid perturbation of the soliton during data acquisition. We again observe from the side of the crystal the scattered light due to the propagating beam. Before soliton formation, diffraction is illustrated by the widening of the beam as it propagates through the crystal [Fig. 4(c)]. When the positive index perturbation generated by a dark soliton is present, the beam narrows within the first few millimeters of the medium, and main-

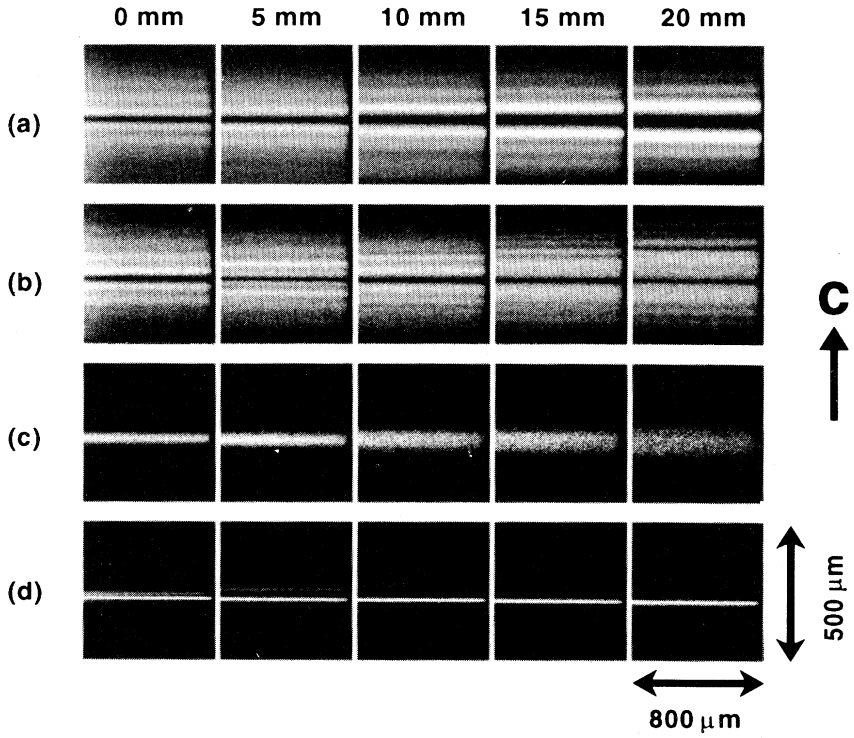

FIG. 4. Properties of a soliton launched into a 1×5 cm^2 sample of congruent $LiNbO_3$. The diameter of the background 488-nm beam is ~0.6 mm, and the average intensity is ~10 W/cm^2. A mosaic of the side view of the 488-nm beam with a phase step is shown (a) for the initial condition before soliton formation and (b) at steady state after soliton formation. A corresponding mosaic of the side view of a separate 514-nm beam launched collinear to the 488-nm beam is shown (c) before soliton formation and (d) as guided by the index perturbation left behind by the 488-nm soliton. The images are obtained at 5-mm intervals and show a width of 800 μm.

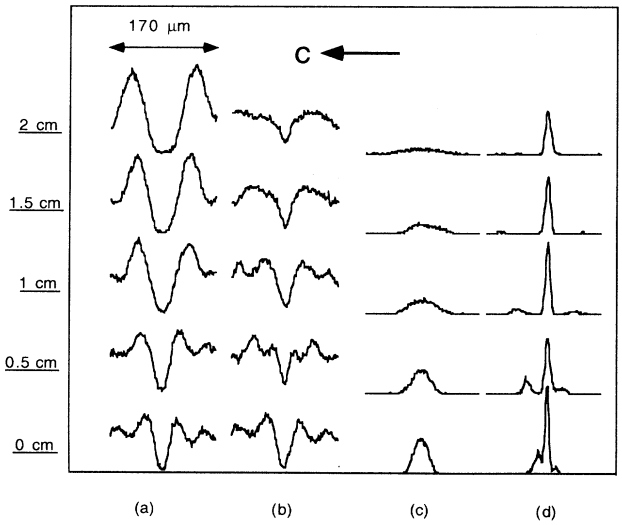

FIG. 5. Profiles of a soliton launched into a $1\times1\times5$ cm^3 sample of congruent $LiNbO_3$. The diameter of the background 488-nm beam is ~0.6 mm, and the average intensity is ~10 W/cm^2. Profiles of the side view of the 488-nm beam with a phase step are shown (a) for the initial condition before soliton formation and (b) at steady state after soliton formation. Profiles of the side view using a separate 514-nm beam are shown (c) before soliton formation and (d) as guided by the index perturbation left behind by the 488-nm soliton. The images are obtained at 5-mm intervals.

tains a relatively uniform profile through the remainder of the medium. Such waveguides persist in the dark [Fig. 4(d)]. The waveguide used to guide the 514-nm beam illustrated here is the same index perturbation responsible for the soliton in Fig. 4(b). The waveguide structure has been observed to persist for a minimum of 39 h in the absence of continuous illumination, and is expected to have a lifetime corresponding to the dark decay time in the sample, which can be on the order of months to years in $LiNbO_3$. With continuous illumination at most visible wavelengths, however, the waveguides formed by photovoltaic solitons eventually decay in the absence of a suitable fixing mechanism.

The profiles of the second wavelength may also be examined to determine whether they show diffraction or guiding. The profiles corresponding to Fig. 4(c) are shown in Fig. 5(c), illustrating significant diffraction from the front surface of the medium. The profiles corresponding to Fig. 4(d) are shown in Fig. 5(d), illustrating guiding of the launched beam after a soliton has been formed at the initial wavelength.

We have observed soliton behavior within an intensity range of 10 mW/cm^2 to 10 W/cm^2, above which we observed optical degradation in the form of large perturbations in the background intensity. The widths do not vary significantly over the range of intensities investigated, and fall within the range of 20 to 30 μm. Although the intensity is significantly larger than the dark irradiance, the observed soliton widths are comparable to the soliton widths predicted for intensity comparable to dark irradiance [13]. The dark notch does not broaden with increasing intensity (as expected from the theory [13]), but instead became grayer. This effect may be due to perturbations at the front surface or perturbations within the medium, which prevent the notch from being completely dark and therefore prevent the nonlinearity from saturating appropriately [13]. The behavior of these perturbations may be further linked to severe beam degradation at high intensities, as originally observed by Ashkin *et al.* [24]. Further theoretical and experimental investigation is required to determine the impact of the finite beam size on the nonlinear dynamics, the difference between open and closed circuit boundary conditions, the impact of different dark irradiances through techniques such as temperature variation to change the dark conductivity directly or illumination with incoherent light to control effective dark conductivity, and the behavior of grey solitons in a defocusing photovoltaic medium.

In summary, we have observed dark planar spatial solitons in a photovoltaic-photorefractive medium. The photovoltaic solitons exhibit tensorial and orientational properties manifested in the dependence of their shape and size on their polarization, direction of propagation and gradient of the amplitude profile, with respect to the principal axes of the crystalline photovoltaic medium. We have shown that the photovoltaic solitons are capable of guiding beams at less sensitive wavelengths and therefore may be used for producing waveguides in the interior of bulk media.

We gratefully acknowledge Y. Furukawa of Hitachi Metals, Ltd., and Crystal Technology, Inc., for growth and preparation of the $LiNbO_3$ sample used in this research, and A. Yariv and B. Crosignani for helpful discussions. M.T., M.C.B., and M.M.F. acknowledge the support of the Advanced Research Projects Agency (ARPA) through the Center for Nonlinear Optical Materials at Stanford University, and Shin-Etsu Chemical Co., Ltd. G.C.V. acknowledges the support of Hughes Aircraft Company Internal Research and Development.

[1] R. Y. Chiao, E. Garmire, and C. H. Townes, Phys. Rev. Lett. **13**, 479 (1964).
[2] V. E. Zahkarov and A. B. Shabat, Zh. Eksp. Teor. Fiz. **61**, 118 (1971) [Sov. Phys. JETP **34**, 62 (1972)].
[3] J. E. Bjorkholm and A. Ashkin, Phys. Rev. Lett. **32**, 129 (1974).
[4] A. Barthelomy, S. Maneuf, and C. Froehly, Opt. Commun. **55**, 201 (1985).
[5] J. S. Aitchison, A. M. Weiner, Y. Silberberg, M. K. Oliver, J. L. Jackel, D. E. Leaird, E. M. Vogel, and P. W. Smith, Opt. Lett. **15**, 471 (1990).
[6] V. E. Zahkarov and A. B. Shabat, Zh. Eksp. Teor. Fiz. **64**, 1627 (1973) [Sov. Phys. JETP **37**, 823 (1973)].
[7] G. A. Swartzlander Jr., D. R. Anderson, J. J. Regan, H. Yin, and A. E. Kaplan, Phys. Rev. Lett. **66**, 1583 (1991).
[8] G. R. Allan, S. R. Skinner, D. R. Anderson, and A. L. Smirl, Opt. Lett. **16**, 156 (1991).
[9] A. W. Snyder, D. J. Mitchell, and B. Luther-Davies, J.

Opt. Soc. Am. B **10**, 2341 (1993).
[10] S. Gatz and J. Herrmann, J. Opt. Soc. Am. B **8**, 2296 (1991).
[11] Y. Chen, Opt. Commun. **90**, 317 (1992).
[12] W. Korlikowski and B. Luther-Davies, Opt. Lett. **18**, 188 (1993).
[13] G. C. Valley, M. Segev, B. Crosignani, A. Yariv, M. M. Fejer, and M. C. Bashaw, Phys. Rev. A **50**, R4457 (1994).
[14] Y. R. Shen, *The Principles of Nonlinear Optics* (John Wiley & Sons, New York, 1984).
[15] A. Yariv, *Optical Electronics,* 4th ed. (Saunders College Publishing, New York, 1991).
[16] M. Segev, B. Crosignani, A. Yariv, and B. Fischer, Phys. Rev. Lett. **68**, 923 (1992).
[17] G. C. Duree Jr., J. L. Shultz, G. J. Salamo, M. Segev, A. Yariv, B. Crosignani, P. DiPorto, E. J. Sharp, and R. R. Neurgaonkar, Phys. Rev. Lett. **71**, 533 (1993).
[18] G. Duree, M. Morin, G. Salamo, M. Segev, A. Yariv, B. Crosignani, and P. DiPorto, Phys. Rev. Lett. **74**, 1978 (1995).
[19] M. Segev, G. C. Valley, B. Crosignani, and P. DiPorto, Phys. Rev. Lett. **73**, 3211 (1994).
[20] M. D. I. Iturbe Castillo, P. A. Marquez Aguilar, J. J. Sanchez-Mondragon, S. Stepanov, and V. Vysloukh, Appl. Phys. Lett. **64**, 408 (1994).
[21] M. Shih, M. Segev, G. C. Valley, G. Salamo, B. Crosignani, and P. DiPorto, Electron. Lett. **31**, 826 (1995).
[22] D. R. Anderson, D. E. Hooton, G. A. Swartzlander, Jr., and A. E. Kaplan, Opt. Lett. **15**, 783 (1990).
[23] B. Luther-Davies and Y. Xiaoping, Opt. Lett. **17**, 496 (1992).
[24] A. Ashkin, G. D. Boyd,, J. M. Dziedzic, R. G. Smith, A. A. Ballman, J. J. Levinstein, and K. Nassau, Appl. Phys. Lett. **9**, 72 (1966).

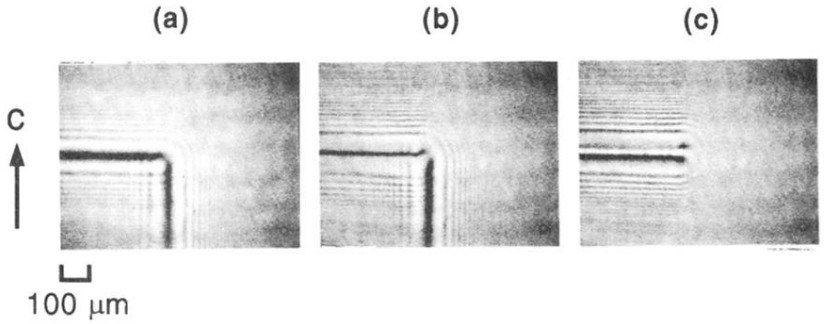

FIG. 3. Orientational behavior of dark photovoltaic solitons for a $1\times1\times1$ cm^3 sample of congruent $LiNbO_3$. The background beam diameter is ~1.4 mm and the average intensity is ~2 W/cm^2. Shown are (a) the initial intensity distribution in the output plane when the corner of the cover slip is in the beam path; (b) intensity distribution at steady state; and (c) intensity distribution after removal of the cover slip immediately after steady state.

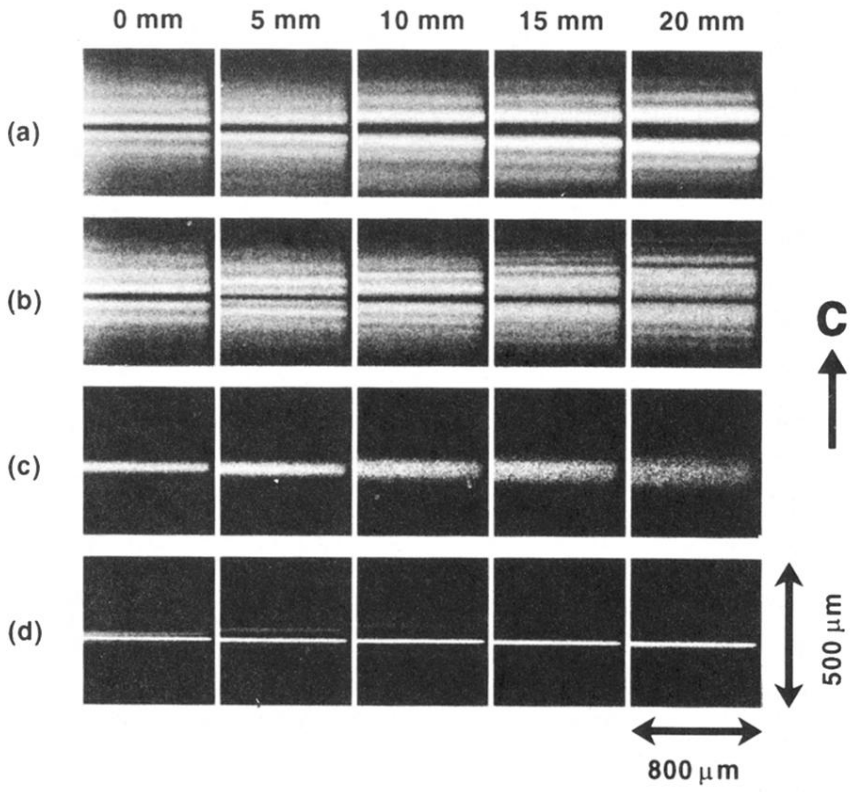

FIG. 4. Properties of a soliton launched into a 1×5 cm^2 sample of congruent $LiNbO_3$. The diameter of the background 488-nm beam is ~0.6 mm, and the average intensity is ~10 W/cm^2. A mosaic of the side view of the 488-nm beam with a phase step is shown (a) for the initial condition before soliton formation and (b) at steady state after soliton formation. A corresponding mosaic of the side view of a separate 514-nm beam launched collinear to the 488-nm beam is shown (c) before soliton formation and (d) as guided by the index perturbation left behind by the 488-nm soliton. The images are obtained at 5-mm intervals and show a width of 800 μm.